Control and Cybernetics

vol. **22** (1993) No. 3

A multilayer computer model for air quality forecasting in urban/regional scale

by

Piotr Holnicki, Andrzej Kałuszko, Antoni Żochowski

Systems Research Institute
Polish Academy of Sciences
PL 01–447 Warsaw
Newelska 6
Poland

The mathematical and computer implementation of a multilayer forecasting model for urban and regional scale is presented. The model has been designed for predicting dispersion and deposition of air pollution in urban and industrial areas and for evaluating the effectiveness of various emission control strategies. The implementation of pollutants dispersion is based on numerical solving the advection-diffusion equations. The wind field is preprocessed by a specialized wind generator. The resulting concentration/deposition distributions are presented in th form of isoline maps. An example of short-term forecast of sulphur dioxide concentration for Warsaw is presented, as a case study.

1. Introduction

Nowadays, air quality analysis is especially important in urban and industrial regions, in view of their high population densities and the numbers of people suffering from its adverse effects on health. Emission fields in these areas are characterized by a variety of species, spatial complexity and high emission intensity. Emissions are mainly due to central or local domestic heating, industrial sources and urban transportation systems. Moreover, in many urban areas, unfavorable topographical and meteorological conditions, "heat island" effect and complex chemical processes that occur in the surface layer of the atmosphere – lead to spatial and temporal accumulation of polluting factors. As a result, pollution concentrations often reach very high values and exceed admissible air quality standards.

Computer forecasting models of air pollution dispersion are powerful tools for environmental impact analysis. Pollution measurements, although giving important reference data, are usually limited to several specific locations. They can be directly utilized in on-line environmental quality monitoring as well as in constructing real time prediction models, Cavarallo, et al (1986), aimed at short-term analysis of air quality and indication of alarm situations.

Another class of air pollution models is based on mathematical description of physical processes of transport, diffusion and chemical transformations. Within this class, there are Gaussian-type models that use the analytical solution of the linearized transport equation from isolated sources as well as models based on numerical solving advection-diffusion equations in complex emission fields, Eliassen, Saltbones (1983), Holnicki, Kałuszko, Żochowski (1992), Juda-Kuczka (1987). Models of this type are very useful in air quality analysis and control in big urban agglomerations and industrial areas.

In this paper a multilayer version of the last group of models is presented. The computer implementation is based on numerical solution of the set of transport equations along with the respective boundary and initial conditions. The real data application for short-term forecasting of SO_2 concentrations in the Warsaw Metropolitan Area is presented.

2. The model description

2.1. Characterization of the input data

The computer implementation is a three-layer version of a mesoscale air pollution forecasting model. The domain considered is a rectangular area of spatial dimensions limited to about 100km x 100km. The dispersion process is analysed in a cuboid limited by terrain elevation and the mixing height – HM. Vertical stratification of this domain consists of three horizontal layers:

- 1st, surface layer 0 – 50m,
- 2nd, middle layer 50 – 150m,
- 3rd, upper layer 150 – HM.

This structure of the model is an approximation of a three-dimensional process and allows us to consider the vertical structure of the wind and the pollutant concentration field. All the ground level, area and linear sources as well as the small pointwise sources are located in the first layer. The strong influence of aerodynamic roughness, turbulence and wind shear are observed at this level. In the second layer most of the emissions of industrial and intermediate energy installations are considered. This is a transfer zone between the highest sources and the ground surface. The effective emission points of the main power and central heating plants are placed in the third layer. The depth of this layer depends on the mixing height and varies both in space and time.

This version of the model is mainly sulphur-oriented but it can be extended to other types of air pollutants. The time scale of the forecast can be optionally

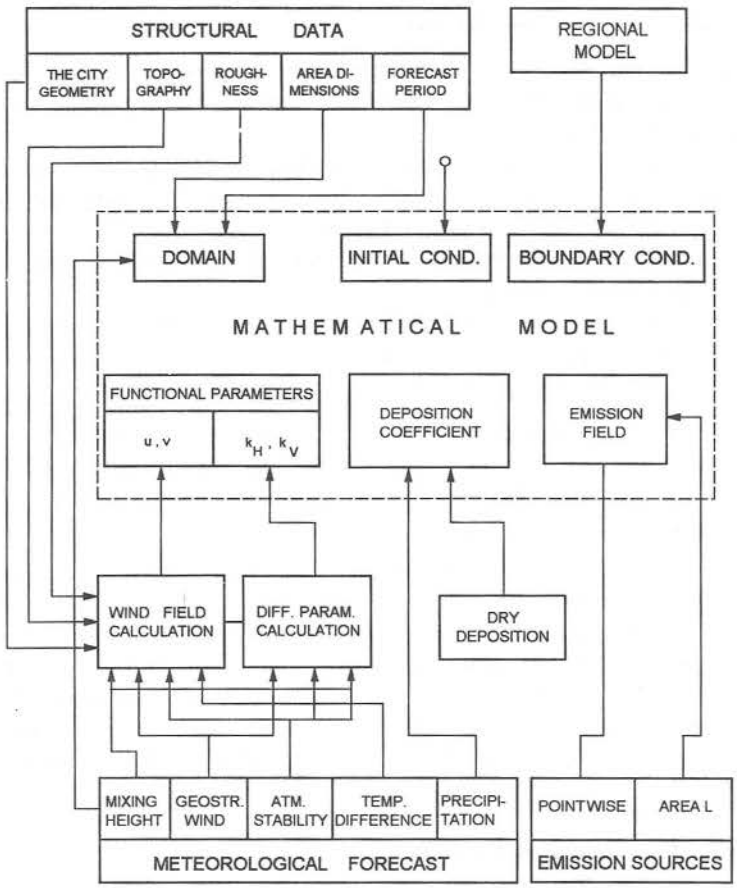

Figure 2.1. The block diagram and the main input data

selected, and ranges from 24 hrs (short-term forecast) up to one year or a season period (long-term forecast). The time horizon is discretized with an interval - DT (in a standard case $DT = 6$hrs). The area considered is discretized with a square mesh. The standard grid length is $\Delta h = 0.5$ - 1km for the urban scale and 2 - 5km for the regional scale.

The main input data utilized by the model are presented in Fig. 2.1. They can be arranged in the following basic groups:

- structural characteristics of the domain of analysis (geometry of the area and its ecological structure, topography and aerodynamic roughness, time horizon of analysis),
- meteorological forecast parameters (mixing height, geostrophic and anemometric wind speed components, precipitation intensity, difference of temperatures between urban and rural areas),
- emission field characteristics (parameters of pointwise emission sources, linear and areal emission flux),
- physical and chemical transformation parameters (dry and wet deposition coefficients, chemical transformation rate),
- initial and boundary conditions.

All the time-dependent data are introduced at the beginning of the current time interval. The results of computation represent SO_2 or $SO_4^=$ concentration maps for short term forecasts. In case of long term prediction, a map of total sulphur deposition is additionally generated.

The model parameters, like diffusion coefficients, chemical transformation rates or wet/dry removal factors are preprocessed in the specified numerical procedures. All the emission functions are transformed into a unified, space distributed emission field. Boundary conditions can be assumed as time-averaged concentration fields, generated by the regional scale model. Computation of the final wind field and simulation of the main dispersion processes are performed in the block *MATHEMATICAL MODEL* which is described in the next section.

2.2. The mathematical background

The emitted compounds are transformed in the course of chemical and physical reactions and are transported during the dispersion processes. The final environmental effect is a result of dry and wet deposition of polluting species as well as the resulting concentration. A general view of the main steps of the sulphur oxides life cycle in the atmosphere is schematically shown in Fig. 2.2, Dernwent (1988), Morgan et al. (1986).

The same form of mathematical model of dispersion process is applied for each layer. It consists of the set of two advection-diffusion equations, for primary and secondary pollutants, respectively, considered in a rectangular domain $\Omega = L_x \times L_y$. Two neighbouring layers are coupled by means of vertical diffusion

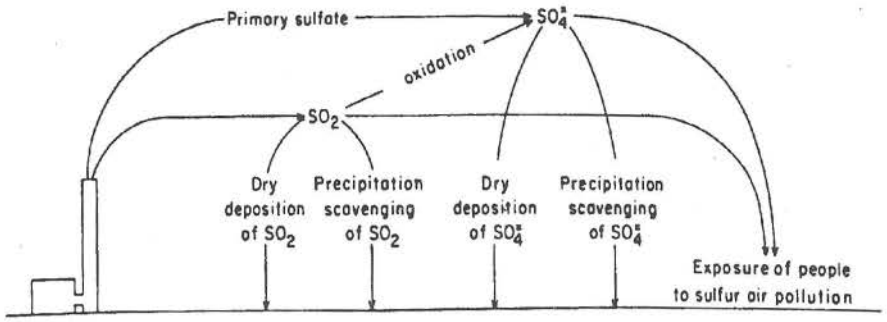

Figure 2.2. The sulphur life cycle and chemical transformations

process.

$$\frac{\partial c_{1,i}}{\partial t} + \vec{w}_i \cdot \nabla c_{1,i} - K_{H_i}\Delta c_{1,i} - \frac{\partial}{\partial z}K_{V_i}\frac{\partial c_{1,i}}{\partial z} + \left(\frac{v_{d_1}}{H_i} + k_{w_1} + k_t\right) c_{1,i} = (1-\beta)\bar{Q}_i, \tag{2.1}$$

$$\frac{\partial c_{2,i}}{\partial t} + \vec{w}_i \cdot \nabla c_{2,i} - K_{H_i}\Delta c_{2,i} - \frac{\partial}{\partial z}K_{V_i}\frac{\partial c_{2,i}}{\partial z} + \left(\frac{v_{d_2}}{H_i} + k_{w_2}\right) c_{2,i} - k_t c_{1,i} = \beta\bar{Q}_i, \tag{2.2}$$

in $\Omega \times (0,T)$, with the boundary conditions ($k = 1,2,\ i = 1,2,3$)

$$c_{k,i} = c^b_{k,i} \text{ on } S^- = \{\partial\Omega \times (0,T) \mid \vec{w}_i \cdot \vec{n} < 0\}, \tag{2.3}$$

$$\frac{\partial c_{k,i}}{\partial \vec{n}} = 0 \text{ on } S^+ = \{\partial\Omega \times (0,T) \mid \vec{w}_i \cdot \vec{n} \geq 0\}, \tag{2.4}$$

and the initial condition ($k = 1,2,\ i = 1,2,3$)

$$c_{k,i}(0) = c^o_{k,i} \text{ in } \Omega \times \{t = 0\}. \tag{2.5}$$

The following notation is assumed:
T – time horizon of the forecast, in $[s]$,
$i = 1,2,3$ – the layer index,
$k = 1,2$ – pollutant type index,
c_1, c_2 – concentration of primary (SO_2) and secondary $(SO_4^=)$ pollutant, in $[\mu g/m^3]$,
H_i – the i-th layer height, in $[m]$,
K_{H_i} – horizontal diffusion coefficient in the i-th layer, in $[m^2/s]$,
K_{V_i} – vertical diffusion coefficient in the i-th layer, in $[m^2/s]$,

$\bar{Q}_i$ – averaged emission field of the i-th layer, in $[\mu g/m^3 s]$,
v_{d_k} – dry deposition velocity for $SO_2\,(SO_4^=)$, in $[m/s]$,
k_{w_k} – wet removal factor for $SO_2\,(SO_4^=)$, in $[1/s]$,
k_t – chemical transformation rate $SO_2 \rightarrow SO_4^=$, in $[1/s]$,
β – relative share of primary sulfate ($SO_4^=$) in emission, in $[-]$,
$\vec{n}$ – the normal outward vector.

In the case of the long-term forecast, the field of total sulphur deposition is calculated. It is expressed as a sum of dry and wet deposition in the consecutive time intervals:

$$D = \sum_{j=1}^{N} [\, D_d(j) + D_w(j) \,], \tag{2.6}$$

where

$$D_d(j) = [\, v_{d_1} c_{1,1}(j) + v_{d_2} c_{2,1}(j) \,] \cdot \Delta t\,,$$

$$D_w(j) = \sum_{i=1}^{3} [\, k_{w_1} c_{1,i}(j) + k_{w_2} c_{2,i}(j) \,] \cdot H_i \cdot \Delta t\,.$$

We denote here $\Delta t = T/N$, and $j = 1, \ldots, N$ is an index of the current time interval.

The horizontal diffusion coefficient in the model layers (for $i = 1, 2, 3$) is calculated by the following relation Holnicki (1990), Juda-Kuczka (1987):

$$K_{H_i} = \sigma_\Theta^2 \cdot max(0.5, |\, \vec{w}_i \,|) \cdot \Delta h, \tag{2.7}$$

where
σ_Θ – the root–mean–square horizontal fluctuation of wind direction, in $[rd]$,
$\vec{w}_i$ – mean wind velocity in the i-th layer, in $[m/s]$,
Δh – space discretization step, in $[m]$.

An essential role in (2.7) is played by the parameter σ_Θ, depending on many factors, such as wind direction and velocity, atmospheric stability, aerodynamic roughness and others Hanna, Briggs, Hosker (1982), Holnicki, Kałuszko, Żochowski (1992). Since all these relations are difficult to describe precisely, in the present version of the model we assume that σ_Θ is a simple function of stability class alone, as shown in Table 2.1.

Table 2.1. Relation σ_Θ versus atmospheric stability class

stability class	A	B	C	D	E	F
σ_Θ	20^o	17.5^o	15^o	12^o	8^o	5^o

The values of dry deposition velocities are adopted from experimental data known from literature, Eliassen, Saltbones (1983), Dernwent (1988), as constant factors. Coefficients of wet removal $k_{w_i}(\alpha)$ that appear in (2.1) and (2.2) are defined as nonlinear functions of precipitation intensity (see Holnicki, Żochowski

(1990)). It also possible to include the seasonal variability of these velocities, as suggested in Eliassen, Saltbones (1983).

The chemical transformation rate k_t depends on many factors, like meteorological conditions, concentration of catalytic species, etc. Holnicki, Zochowski (1990), Juda-Kuczka (1987), but for algorithmic simplicity, we assume a constant value in this implementation. The ranges of main parameters utilized in the model are collected in Table 2.2.

Table 2.2. The default values of main model parameters

Parameter notation		Range/Quantity	Unit
Space dimensions	$L_x \times L_y$	100x100	km
Discretization step	Δh	$0.5 - 5$	km
Time horizon	T	$1 - 365$	day
Time step	ΔT	6	$hour$
Mixing height	HM	$HM(t)$	m
Wind field	$\vec{w}$	generated	m/s
Diffusion coefficients	K_H, K_V	parametrized	m^2/s
Dry deposition SO_2	v_{d_1}	$8 \cdot 10^{-3}$	m/s
Dry deposition $SO_4^=$	v_{d_2}	$2 \cdot 10^{-3}$	m/s
Wet removal SO_2	k_{w_1}	$k_{w_1}(\alpha)$	$1/s$
Wet removal $SO_4^=$	k_{w_2}	$k_{w_2}(\alpha)$	$1/s$
Transformation rate	k_t	variable	$1/s$
Precipitation	α	$\alpha(t)$	mm/h
Atmospheric stability	s	$1 - 6$	–
Primary sulfate emission	β	0.05	–

A parametrization of initial plume rise in the neighbourhood of high stacks (power plants, heating plants, major industrial sources) is applied. The method is based on the downwind shift of the effective emission point, according to the stack parameters and the actual meteorological conditions. The algorithm is based on the specialized instructions Chróściel (ed.) (1983), concerning routine calculation of pollutant concentration in the neighbourhood of the isolated industrial sources. The details of the parametrization can be found in Holnicki (1990).

3. Multi-layer wind field approximation

3.1. The vertical wind profile and topographical corrections

Horizontal transport of air pollution is mainly due to the advection process; thus the calculation of the wind field components in (2.1) and (2.2) plays an essential role. Air flow is considered in a cubic domain, limited by the inversion base –

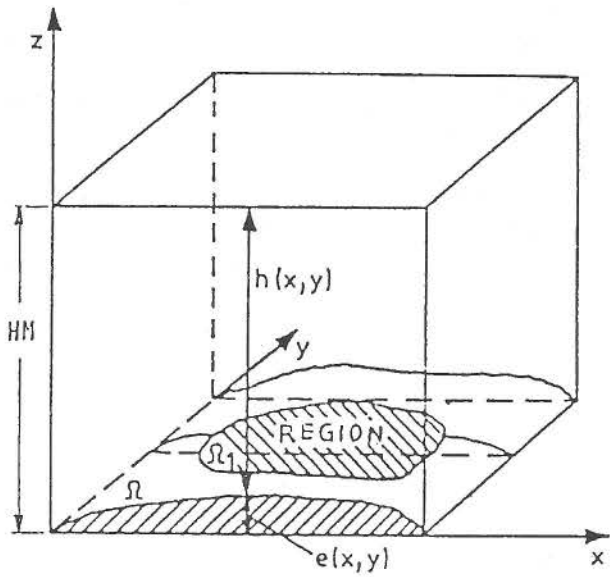

Figure 3.1. The domain of wind field calculation

HM and the ground elevation $z = e(x, y)$ (see Fig. 3.1). In the algorithm applied, the following factors are taken into account:

- vertical wind profile (wind shear),
- topography and aerodynamic roughness,
- heat island effect.

For computational efficiency of the final algorithm, we assume linearity of the system. In the approach applied, all the above effects are analysed separately and then the results are superimposed on each other to give the final form of the wind field in the area.

In the first step, the layer-averaged wind components $\bar{u}_o^i$, $\bar{v}_o^i$ are calculated for $(i = 1, 2, 3)$

$$\bar{u}_o^i = \frac{1}{H_i} \int_{z_{i-\frac{1}{2}}}^{z_{i+\frac{1}{2}}} u_o(z)\, dz, \qquad \bar{v}_o^i = \frac{1}{H_i} \int_{z_{i-\frac{1}{2}}}^{z_{i+\frac{1}{2}}} v_o(z)\, dz, \tag{3.1}$$

where $(z_{i-\frac{1}{2}}, z_{i+\frac{1}{2}})$ is the i-th layer depth and the vector (u_o, v_o) is the solution of the set of generalized Ekman equations Holnicki, Żochowski (1990)

$$\begin{aligned} \frac{\partial}{\partial z}(K_M(z)\frac{\partial u_o}{\partial z}) + \rho f v_o &= \rho f v_g, \\ \frac{\partial}{\partial z}(K_M(z)\frac{\partial v_o}{\partial z}) - \rho f u_o &= \rho f u_g \end{aligned} \tag{3.2}$$

with the boudary conditions

$$u_o(\bar{e}) = u_a, \quad v_o(\bar{e}) = v_a,$$
$$u_o(HM) = u_g, \quad v_o(HM) = v_g.$$

Vectors (u_g, v_g) and (u_a, v_a) represent here geostrophic and anemometric winds, respectively, $\bar{e}$ – the average ground elevation over Ω , f – Corriolis parameter, K_M – the vertical function depending on atmospheric stability Hanna, Briggs, Hosker (1982), Uliasz (1983).

In the next step, the influence of topography and surface roughness is considered. We want to find the minimal corrections $\delta_t\bar{u}$ and $\delta_t\bar{v}$ to the mixing layer averaged components – $\bar{u}_o$, $\bar{v}_o$, such that the modified wind vector

$$[\bar{u}\,,\,\bar{v}\,] = [\,\bar{u}_o + \delta_t\bar{u}\;,\;\bar{v}_o + \delta_t\bar{v}\,]$$

satisfies the conservation law

$$\frac{\partial\bar{u}}{\partial x} + \frac{\partial\bar{v}}{\partial y} = 0.$$

The problem is equivalent to the minimization of the functional

$$L(\delta_t\bar{u}, \delta_t\bar{v}; \lambda) = \int_\Omega [(h\delta_t\bar{u})^2 + (h\delta_t\bar{v})^2 + \lambda(\frac{\partial(h\bar{u})}{\partial x} + \frac{\partial(h\bar{u})}{\partial y})]ds\,, \tag{3.3}$$

where $h(x,y) = HM - e(x,y)$, and λ is the Lagrange multiplier related to the conservation equation constraint.

It can be shown, Dickerson (1978), that the minimum of (3.7) occurs for

$$\delta_t\bar{u} = \frac{1}{2h}\cdot\frac{\partial\lambda^*}{\partial x}, \quad \delta_t\bar{v} =\cdot \frac{1}{2h}\cdot\frac{\partial\lambda^*}{\partial y}\,, \tag{3.4}$$

where the optimal value of Lagrange multiplier – λ^* is the solution of the following Dirichlet problem:

$$\begin{aligned} \Delta\lambda &= -\bar{u}_o\frac{\partial h}{\partial x} - \bar{v}_o\frac{\partial h}{\partial y} \quad \text{in } \Omega\,, \\ \lambda &= 0 \qquad\qquad\qquad\quad \text{on } \partial\Omega\,. \end{aligned} \tag{3.5}$$

Any solution λ^* can be expressed as a linear combination of functions $\lambda(1,0)$ and $\lambda(0,1)$. These are the solutions to (3.5) for $[\bar{u}_o, \bar{v}_o] = [1,0]$ and

$[\bar{u}_o, \bar{v}_o] = [0,1]$, respectively. Finally, due to superposition principle, the topographic corrections (3.9) can be expressed as

$$\begin{aligned} \delta_t \bar{u} &= \frac{1}{2h}[\bar{u}_o \frac{\partial}{\partial x}\lambda(1,0) + \bar{v}_o \frac{\partial}{\partial x}\lambda(0,1)], \\ \delta_t \bar{v} &= \frac{1}{2h}[\bar{u}_o \frac{\partial}{\partial y}\lambda(1,0) + \bar{v}_o \frac{\partial}{\partial y}\lambda(0,1)]. \end{aligned} \tag{3.6}$$

Note, that the most time consuming part of solving the problem – computation of $\lambda(0,1)$ and $\lambda(1,0)$ – can be performed off-line.

In the last step, the "heat island" effect is considered. Let $\Omega_1 \subset \Omega$ be the area of the city, and let Θ_1, Θ_0 denote the ground level temperatures in Ω_1 and on $\partial\Omega$, respectively.

It can be shown Findlay, Hirt (1969) that the thermal wind corrections are of the form

$$\delta_\Theta \bar{u} = \frac{A}{\Delta h} \cdot \frac{\partial \phi}{\partial x}, \qquad \delta_\Theta \bar{v} = \frac{A}{\Delta h} \cdot \frac{\partial \phi}{\partial y}, \tag{3.7}$$

where A, Δh are constant parameters and ϕ is a thermal potential, such that

$$\begin{aligned} \Delta\phi &= (\Theta_g - \bar{\Theta}_g) \qquad \text{in } \Omega, \\ \phi &= 0 \qquad\qquad\quad \text{on } \partial\Omega. \end{aligned} \tag{3.8}$$

By Θ_g we denote here the ground level temperature distribution, and $\bar{\Theta}_g$ is the same temperature, averaged over Ω.

To solve (3.8) we must find Θ_g distribution in Ω. For simplicity, we assume a constant value $\Theta_g = \Theta_1$ in Ω_1. Hence, it is enough to solve the problem

$$\begin{aligned} \Delta\Theta_g &= 0 \quad \text{in } \Omega - \Omega_1, \\ \Theta_g &= \Theta_0 \quad \text{on } \partial\Omega, \\ \Theta_g &= \Theta_1 \quad \text{on } \partial\Omega_1, \end{aligned} \tag{3.9}$$

Here again we apply superposition principle. Let $\phi(1)$ be the reference solution of (3.8), (3.9) for $\Theta_0 = 0$ and $\Theta_1 = 1$. Then, for the current value of the difference of temperatures,

$$\phi = (\Theta_1 - \Theta_0) \cdot \phi(1)$$

and, by (3.7), the final form of thermal corrections is

$$\begin{aligned} \delta_\Theta \bar{u} &= \frac{A}{\Delta h}(\Theta_1 - \Theta_0)\frac{\partial \phi(1)}{\partial x}, \\ \delta_\Theta \bar{v} &= \frac{A}{\Delta h}(\Theta_1 - \Theta_0)\frac{\partial \phi(1)}{\partial y}, \end{aligned} \tag{3.10}$$

where $\phi(1)$ and the derivatives $\partial\phi(1)/\partial x$ and $\partial\phi(1)/\partial y$ can be calculated off-line.

To transform these general corrections to the respective vertical layers we introduce the scaling factor that reflects the parabolic character of the vertical profile of the wind vector module in the mixing layer. We use this factor in the form

$$\alpha_i = \left[\frac{h_{aver} - z_i}{h_{aver}}\right]^2, \tag{3.11}$$

where h_{aver} is the averaged effective depth of the mixing layer. Thus, the total wind components in the respective vertical layers are calculated from (3.1), (3.6), (3.10) and are expressed as

$$\begin{aligned} \bar{u}^i &= \bar{u}^i_o + \alpha_i\,(\,\delta_t\bar{u} + \delta_\Theta\bar{u}), \\ \bar{v}^i &= \bar{v}^i_o + \alpha_i\,(\,\delta_t\bar{v} + \delta_\Theta\bar{v}), \end{aligned} \tag{3.12}$$

for $i = 1, 2, 3$ and depend on space coordinates.

3.2. Interpolation of the measurement wind data

In general, besides the global meteorological forecast (like the mixing layer height and geostrophic wind, precipitation, etc.) given for the entire computational domain, there exist measurement data, recorded in a number of meteorological stations located in a given area. These data concern the observed values of the ground level (anemometric) wind components and can be extrapolated for the following time interval. This additional information is utilized in the algorithm of the wind-field generation by spatial interpolation of the measurement data.

The principal difficulty in flow modelling (particularly wind field modelling) is reaching a compromise between the inherently complicated nature of the phenomenon and the requirement of the admissibility of the computational procedure. In this case we assume that the pressure is harmonic. The interpolation algorithm utilizes two sets of basis functions (see Holnicki, Kałuszko, Żochowski (1992) for details).

The fundamental solutions of Laplace equations for wind components

$$\phi_1 = x \ln r, \tag{3.13}$$

$$\phi_2 = y \ln r. \tag{3.14}$$

are taken as the *basis functions of the first kind* with the centre at (0,0). Here r denotes, as usually, the norm of the current point.

There exist also *basis functions of the second kind* representing the vertices,

$$\psi_1 = -\frac{y}{r}, \tag{3.15}$$

$$\psi_2 = \frac{x}{r}. \tag{3.16}$$

It is easily seen that the basis function satisfy the flow continuity constraint.

Given a certain number of measurements, the procedure of obtaining the interpolated wind field consists of the following steps:

1° At each data point we compute the vertical wind profile by solving the generalized Ekman equations (3.2) for the local meteorological data. Next we compute at every point values of the wind components at heights corresponding to the centres of layers into which the general model divides the volume of the air. In this way three (or more) separate sets of measurements are obtained, one for each level. The next steps of the procedure are performed for every layer separately.

2° We construct nb basis functions of the first and second kind with the centres distributed uniformly on the circle with the middle at the centre of gravity of the computational rectangle and the radius equal to half of the circumference.

3° Using the least squares method we calculate the coefficients in the linear combinations of basis functions approximating the measurement data. Here we may possibly regularize the procedure by introducing the artificial measurements, located in the corners of the rectangle, with values equal to the average of the real data and certain small weights. This is necessary in cases when the measurements are very scarce or are concentrated in a small region. In our program, on the basis of numerical experiments, we take the values $nb = 12$ and the regularizing weights 0.25.

3.3. Merging the theoretical and measured wind fields

Let the vector field $\bar{\mathbf{w}}$ represent the theoretical wind computed using global topographical and meteorological data and $\hat{\mathbf{w}}$ be the interpolated field generated on the basis of mesurements taken at points $\mathbf{p}_i$, $i = 1, ..n$. The final construction rests on the idea, that in the region where data are dense, the resulting field should follow the measurements, while in other regions it should conform to our notion of the theoretically correct behaviour.

To this end we construct the function of the form:

$$g(x, y) = \sum_i \exp(-\alpha|\mathbf{p} - \mathbf{p}_i|),$$

calculate its maximum over the domain – g_{max} , and then define the weight function as

$$\rho(x, y) = g(x, y)/g_{max} . \tag{3.17}$$

Finally, we combine the theoretical and interpolated wind fields according to the formula

$$\mathbf{w}(x, y) = (1 - \rho(x, y))\bar{\mathbf{w}} + \rho(x, y)\hat{\mathbf{w}}. \tag{3.18}$$

The coefficient α must be selected empirically, but according to our experience it should be equal to the inverse of approximately one tenth of the longest side of the computational rectangle.

The procedure described above is illustrated by the example of real measurement data and topography of the region around Teplice, Northern Bohemia, Czech Republic. The terrain is very diversified, with big elevation differences reaching 800 m. Some computational results are presented in figures 3.2 – 3.3. The 15 observation sites are marked by the circles, imposed on the topography map of the terrain. The anemometric and geostrophic winds, measured at each site, are transformed into the respective layer wind vectors (the vertical wind shear effect can be seen). In Fig. 3.2 the average wind blows from the south-east direction. Since the flow is nearly perpendicular to the valley, its influence is not very evident. However, one can see the splitting of stream lines around the hills. In Fig. 3.3 the wind is more parallel to the valley and the channelling effect can be observed.

Two features of the approximation method are evident even from these examples. First, the procedure has a smoothing effect on the theoretical wind field. Without merging with interpolated values, the influence of the topography would be more evident. It means also, that only big scale characteristics of the flow may be predicted. Moreover, the measurements may completely mask the effect of topography if they contain very big errors. However, in experiments when the measurements were created artificially using theoretical model with added small random error, the interpolation itself reproduced the wind field quite well.

4. The computational algorithm

The numerical algorithm applied for solving the multi-layer transport equations is based on the sequential use of a single layer procedure for the consecutive model layers. In the next step, the exchange between layers is performed. The numerical method applied for solving the horizontal transport equations is based on a discrete in time approximation to (2.1) – (2.5) by a combination of the method of characteristics and the finite element technique, Bercovier, Pirroneau, Sastri (1983), Holnicki, Żochowski (1990). Since the same approach is applied to both equations, in the sequel we consider only the first of them (the layer index is omitted for simplicity).

For an urban scale area analysed, the space discretization step can range from 0.5km up to 1km, while on a regional scale the range is 2 – 5km. In this case, the turbulent diffusion process is a subscale effect. Thus, the standard methods of approximation can generate strong 'numerical diffusion' effect that can be of the same order of magnitude as the physical diffusion. To eliminate this drawback, we split the original equation according to advection and diffusion

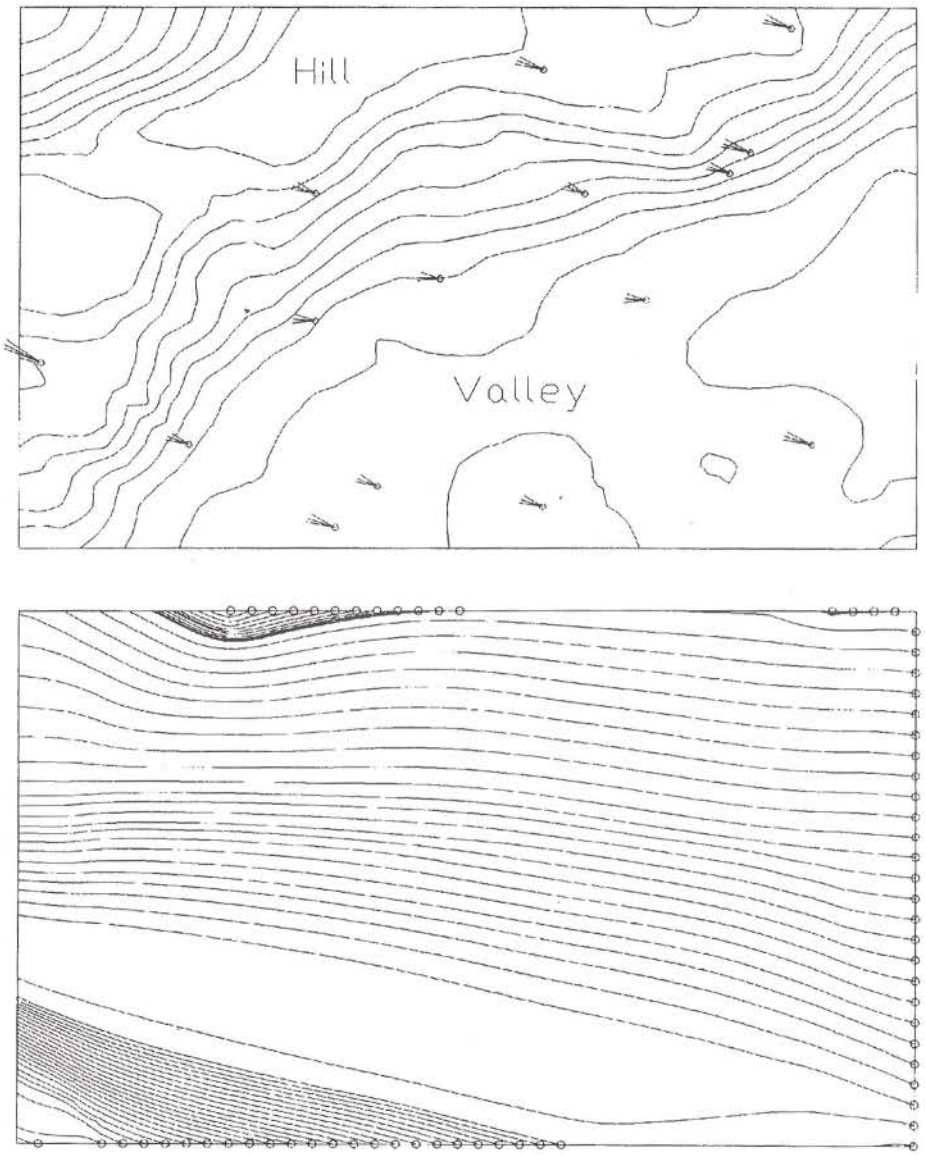

Figure 3.2. The observation data (top) and the calculated streamlines (bottom) for south-east wind direction

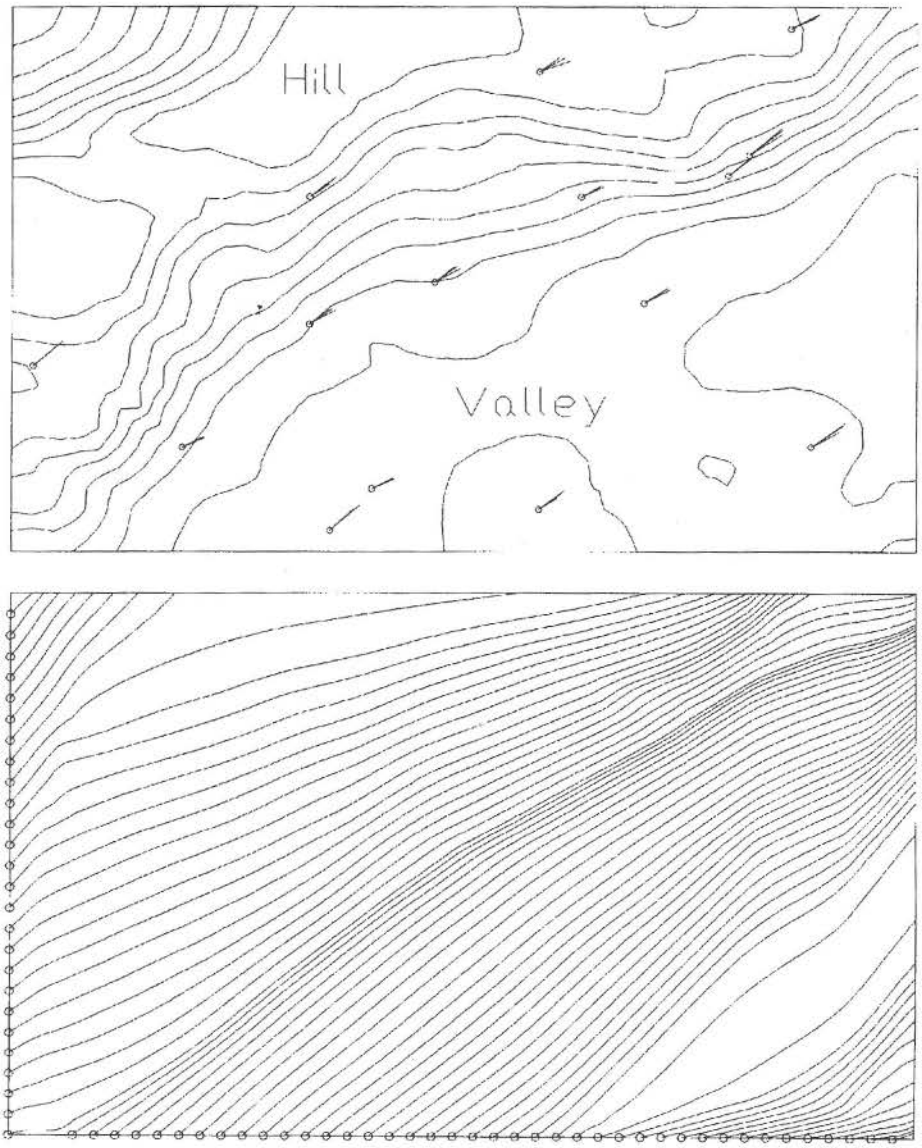

Figure 3.3. The observation data (top) and the calculated streamlines (bottom) for south-west wind direction

processes:

$$\frac{\partial c}{\partial t} + \vec{w} \cdot \nabla c + (\frac{v_d}{HM} + k_w - k_t)c = Q, \tag{4.1}$$

$$\frac{\partial c}{\partial t} - K\Delta c = 0, \tag{4.2}$$

and then we apply different numerical approaches for solving each of them.

The finite-dimensional approximation is directly applied to the first equation. The solution, in the consecutive time steps, is then used as an initial distribution for diffusion equation (4.2). Its analytical solution is next utilized to evaluate dispersion effect in the current time step.

Now we consider approximation of (4.1). In the first step, the equation is split down according to space variables, into an equivalent set of one-dimensional equations. This set, written in a weak form, is as follows:

$$\begin{aligned}
&(\psi_x \tfrac{\partial z}{\partial r}(t)\,,\,\phi) + \sigma(z(t)\,,\,\phi) = \tfrac{1}{2}(F(t)\,,\,\phi),\\
&\quad \forall \phi \in H^1(0, L_x),\ t \in (t_n, t_{n+1}),\ (z(t_n)\,,\,\phi) = (c(t_n)\,,\,\phi)\,,\\
&(\psi_y \tfrac{\partial c}{\partial s}(t)\,,\,\phi) + \sigma(c(t)\,,\,\phi) = \tfrac{1}{2}(F(t)\,,\,\phi),\\
&\quad \forall \phi \in H^1(0, L_y),\ t \in (t_n, t_{n+1}),\ (c(t_n)\,,\,\phi) = (z(t_{n+1})\,,\,\phi)\,,
\end{aligned} \tag{4.3}$$

where $\psi_x = \sqrt{1+u^2}, \psi_y = \sqrt{1+v^2}$ and $r = r(x)$, $s = s(y)$ are characteristic directions related to the operators

$$\frac{\partial}{\partial r} = (\frac{\partial}{\partial t} + u\frac{\partial}{\partial x})/\psi_x\,, \quad \frac{\partial}{\partial s} = (\frac{\partial}{\partial t} + v\frac{\partial}{\partial y})/\psi_y\,.$$

Here F – denotes the emission field, $(\cdot\,,\,\cdot)$ – is a scalar product in the space $L^2(0, L_x)$ (or in $L^2(0, L_y)$, respectively), and

$$\sigma = \frac{v_{d_i}}{HM} + k_{w_i} + k_t\,, \quad (i = 1, 2)\,.$$

Now we define the finite-dimensional approximation to (4.3). Let, for the step of discretization h converging to zero, $V_h = \{v_h\}$ be a linear finite element subspace of $H^1(0, L_x)$ (or $H^1(0, L_y)$), respectively. By $\tau = T/N(\tau)$ we denote time discretization step. Set (4.3) is approximated by the following, discrete-time

Galerkin scheme:

$$
\begin{aligned}
&(\tfrac{z_h^{n+1}-\bar{c}_h^n}{\tau}\,,\,v_h)+\sigma\cdot(z_h^{n+1}\,,\,v_h)=\tfrac{1}{2}(f_h^{n+1}\,,\,v_h)\,,\\
&\qquad\qquad\forall\, v_h\in V_h,\ n=0,1,\ldots,N-1,\\
&(z_h^o\,,\,v_h)=(c_h^o\,,\,v_h)\,,\qquad \forall\, v_h\in V_h\,,\\
&(\tfrac{c_h^{n+1}-\bar{z}_h^n}{\tau}\,,\,v_h)+\sigma\cdot(c_h^{n+1}\,,\,v_h)=\tfrac{1}{2}(f_h^{n+1}\,,\,v_h)\,,\\
&\qquad\qquad\forall\, v_h\in V_h,\ n=0,1,\ldots,N-1,\\
&(c_h^o\,,\,v_h)=(z_h^{n+1}\,,\,v_h)\,,\quad \forall\, v_h\in V_h\,,
\end{aligned}
\tag{4.4}
$$

along with the respective boundary conditions that approximate (2.3) – (2.4).

The horizontal diffusion is governed by the equation (4.2). The applied parametrization method is based on evaluation of the total amount of the i-th layer pollution, being transferred to the neighbouring grid cells in the course of a single time step – τ. This amount is evaluated on the analytical solution to (4.2), see Zdanski A.K., Krylova T.O. (1986), Holnicki (1990). A similar approach is utilized in the parametrization of vertical dispersion.

The direct approximation of the vertical diffusion process requires respectively fine discretization of the equation

$$\frac{\partial c_i}{\partial t} - K_{V_i}\frac{\partial^2 c_i}{\partial z^2} = 0. \tag{4.5}$$

where $i = 1,2,3$ denotes the layer index. In case of a multilayer model, dispersion is a subscale effect and has to be parametized. The amount of the i-th layer pollution, being transferred to the neighbouring layers in course of the single time step – τ, is calculated from the analytical solution to (4.5)

$$c_i(z\,,\,t) = \frac{1}{\sqrt{t}}\cdot exp(-\frac{z^2}{4K_{V_i}t})\cdot c_i\,(z_o,0), \tag{4.6}$$

where $c_i\,(z_o,0)$ is the initial concentration and z_o – the average height of the layer,

$$c_i\,(z_o,0) = c^o\cdot\delta(z-z_o). \tag{4.7}$$

Thus, the resulting vertical transfer of the pollutant depends on the layer height, time discretization step and the vertical diffusion coefficient – K_{V_i}. The quantitative evaluation of this process can be expressed by the coefficient $\gamma_{i,j}$ (the detailed definition can be found in Holnicki, Kałuszko, Żochowski (1992)). Moreover, the intensity of vertical exchange of pollutant between layers depends

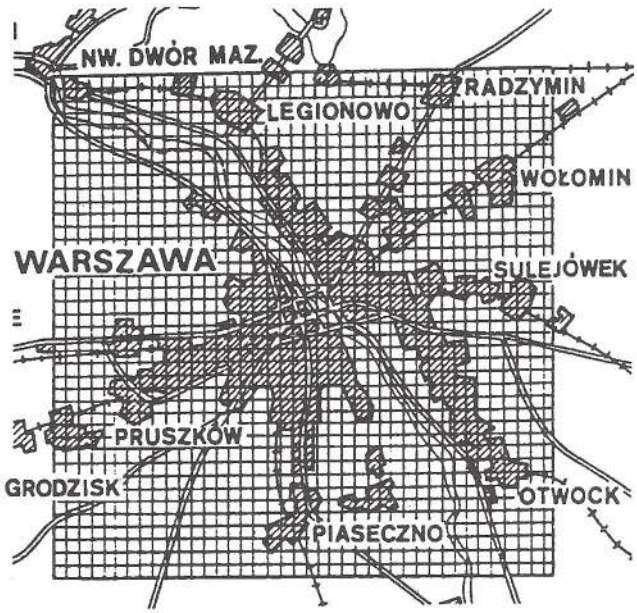

Figure 4.1. The considered urban area

on the current difference of concentrations and can be calculated as follows:

$$\begin{aligned} c_{k,1}(x,t+\tau) &= c_{k,1}(x,t) + \gamma_{1,2}(c_{k,2}(x,t) - c_{k,1}(x,t)), \\ c_{k,2}(x,t+\tau) &= c_{k,2}(x,t) - \gamma_{1,2}(c_{k,2}(x,t) - c_{k,1}(x,t)) + \\ &\quad + \gamma_{2,3}(c_{k,3}(x,t) - c_{k,2}(x,t)), \\ c_{k,3}(x,t+\tau) &= c_{k,3}(x,t) - \gamma_{2,3}(c_{k,3}(x,t) - c_{k,2}(x,t). \end{aligned}$$

This operation is performed as the final step of the numerical algorithm, in the consecutive intervals.

5. The real data application

The model has been implemented in the real data case for short-term forecasting SO_2 concentrations in the Warsaw Metropolitan Area. The region considered is a square $40km \times 40km$ containing the city and the rural area (see Fig. 5.1). In the standard case, this domain is discretized with the square mesh, where $\Delta h = 1km$ step size is applied. The same spatial resolution is used for all the space-dependent input data (emission field, wind field, dispersion parameters etc.).

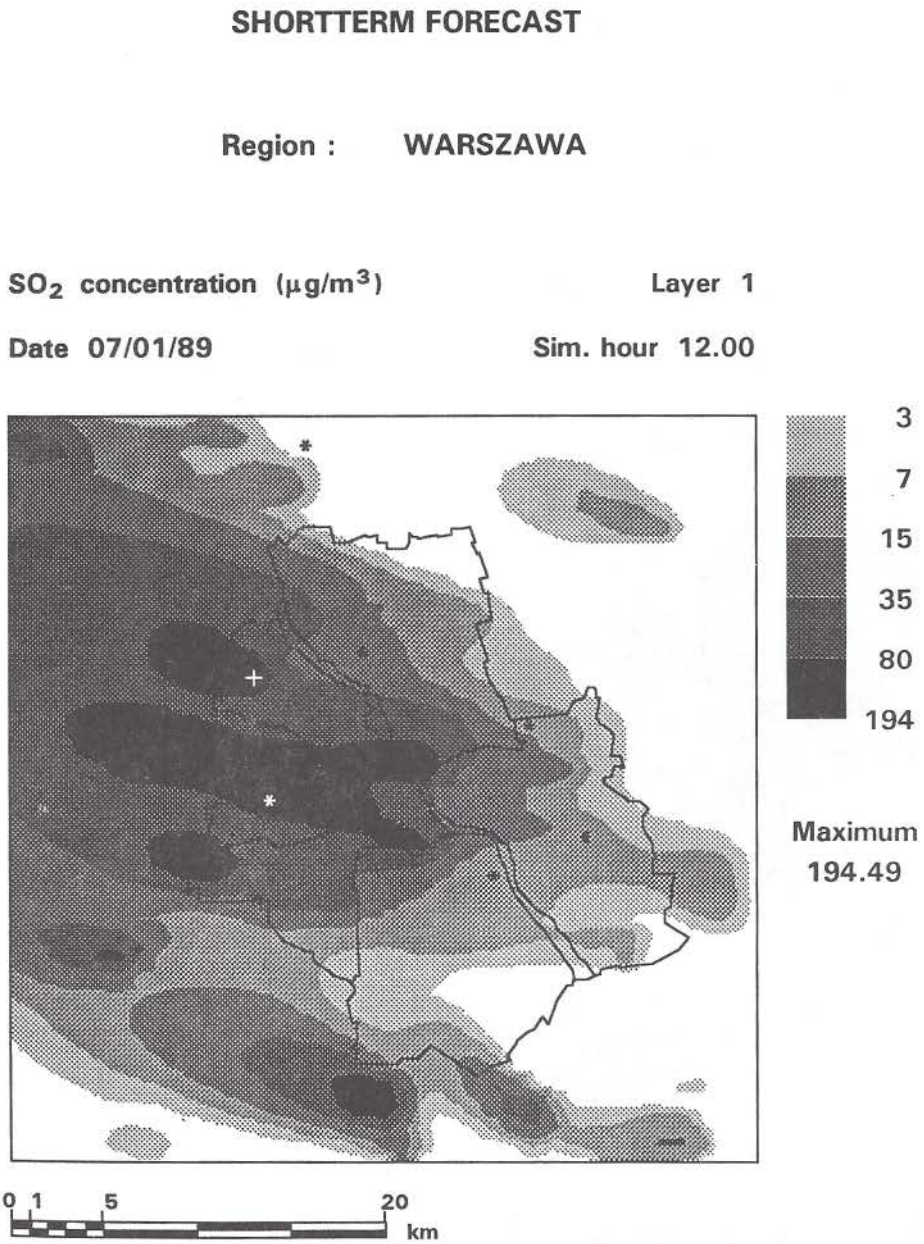

Figure 5.1. A map of SO_2 concentration – layer 1; the values in $[\mu g/m^3]$.

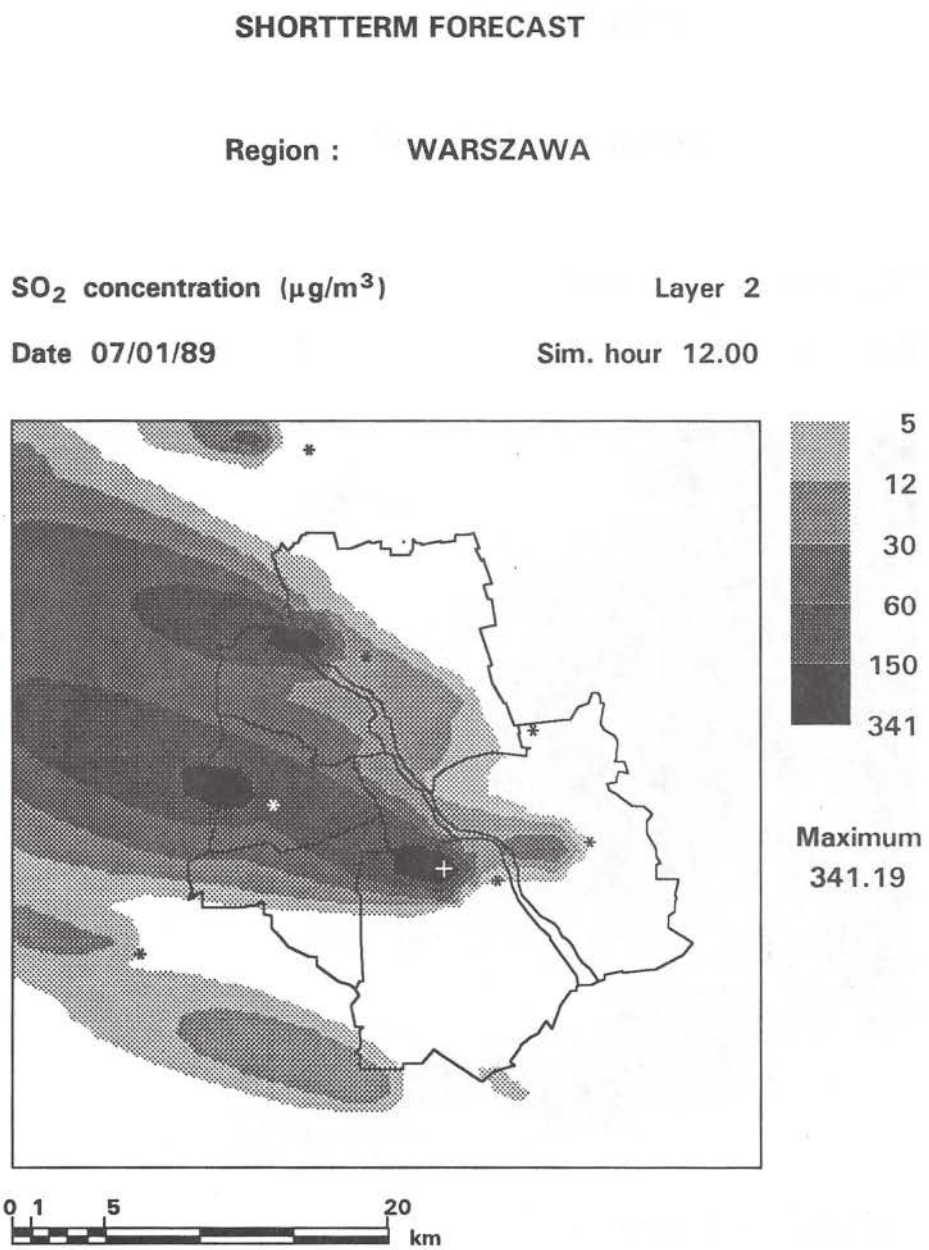

Figure 5.2. A map of SO_2 concentration – layer 2; the values in $[\mu g/m^3]$

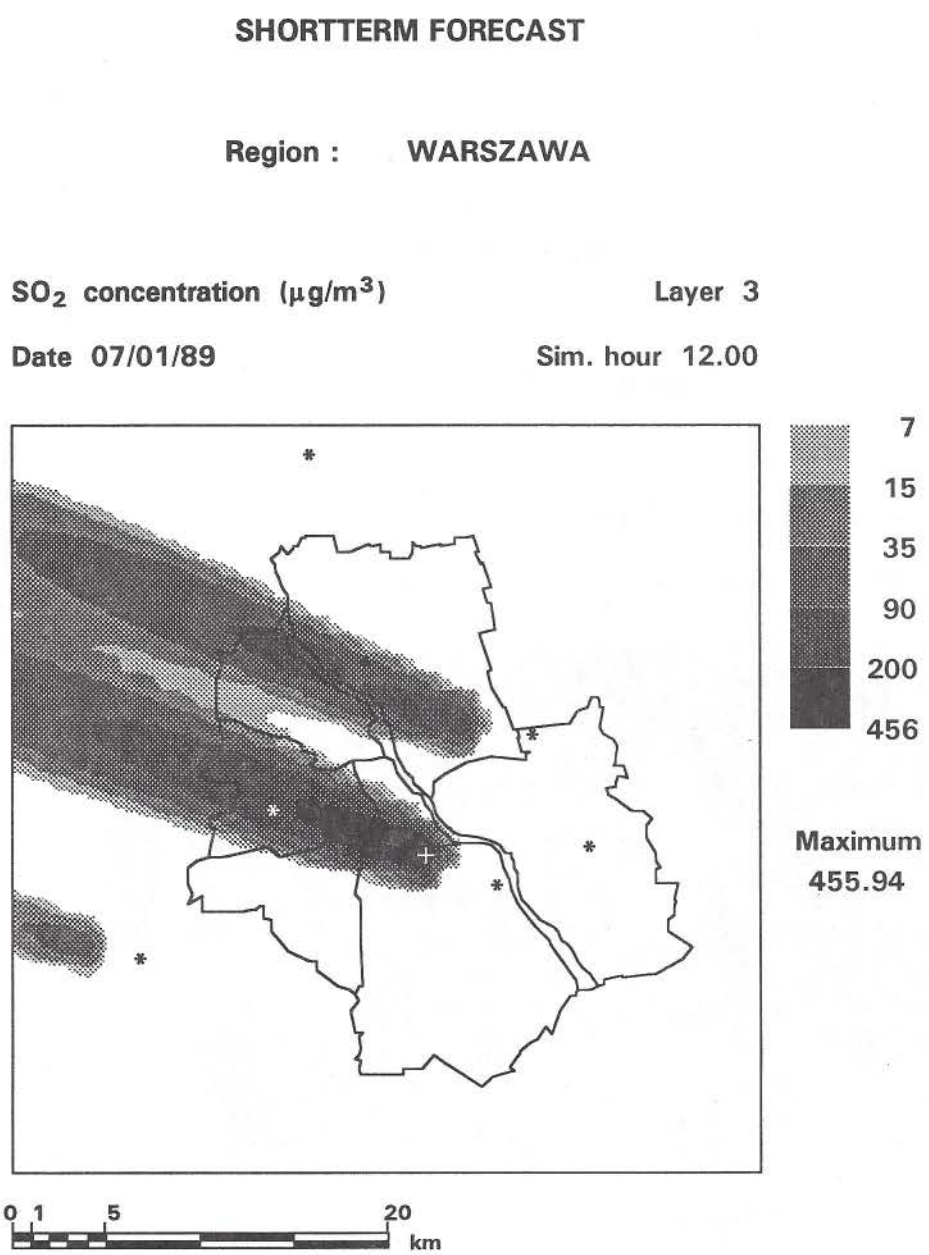

Figure 5.3. A map of SO_2 concentration – layer 3; the values in $[\mu g/m^3]$

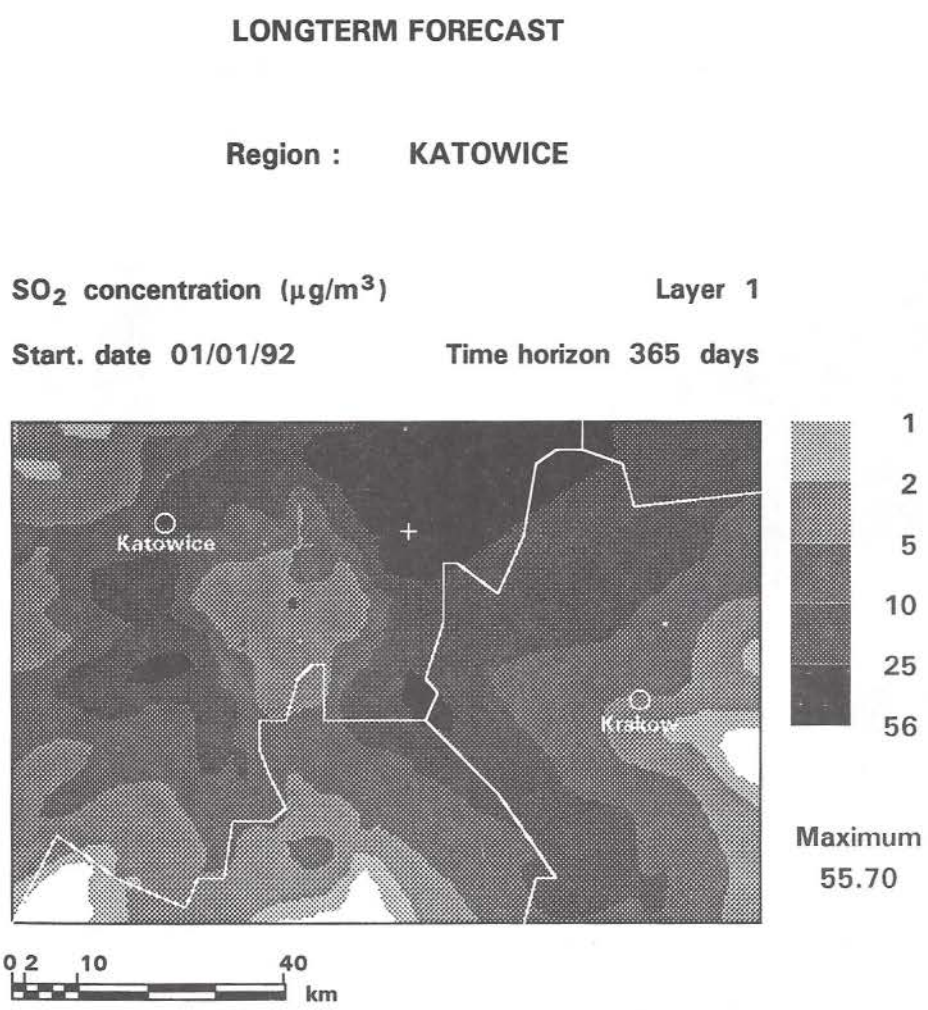

Figure 5.4. Averaged surface-level SO_2 concentration, generated by JaworznoIII power plant, for the winter season

The emission field is constituted by 6 major central heating plants as well as more than 300 intermediate or small heating installations and industrial sources. Moreover, 65 aggregated area sources are considered; they represent domestic heating installations of the main city quarters or suburban districts.

Below, an example of one 6-hour step of a short-term forecast is presented. The resulting maps of SO_2 concentration in the model layers have been generated for south-east weak wind, neutral stability conditions and inversion base height HM = 700m. Figures 5.2 – 5.4 present concentration maps in the bottom, middle and the upper layers, respectively. The surface concentration is mainly due to the ground level sources; the influence of the major power plants is observed at some distance from the position of the main stacks (marked by the stars), depending on the stack parameters, the wind speed and atmospheric stability conditions.

The dynamics of the model can also be important in analysis of long range scenarios. In such a case, the process of transition between the consecutive meteorological situations is continuously simulated and therefore can be reflected in the resulting time-averaged pollution field. An example of long-term environmental analysis is presented in Fig. 5.5. The season-averaged, ground level SO_2 concentration map represents environmental effect of Jaworzno III power plant in Silesia-Kraków Region (110km x 74km). The map is related to the winter season averaged concentrations, obtained for a representative year (from the viewpoint of meteorological conditions). The simulation was performed as a sequence of the consecutive 6-hr meteorological episodes that cover the total period of simulation. The isoline map, besides the meteorological conditions, reflects the influence of source parameters (the stack height, diameter, the outlet gasses temperature and velocity). One can see, for example, relatively low concentrations in some neighbourhood of the source; the maximum concentration area indicates the dominating wind directions in the season considered.

The computer model presented in the paper can be applied as decision support tool in regional planning, evaluating environmental damage of industrial sources, optimal location of new installatins, or optimal strategy selection of emission abatement program. Some examples of these applications can be found in Holnicki, Żochowski (1990), Holnicki, Kałuszko, Żochowski (1992), Holnicki, Kałuszko (1992). Dynamics of the advection-diffusion solver can be also utilized in real-time emission control Holnicki, Żochowski (1990).

References

BERCOVIER M., PIRRONEAU P., SASTRI V. (1983) *Finite elements and characteristics for some parabolic-hyperbolic problems.* Appl. Math. Modelling, vol. 7, April 1983, 89 – 96.

CAVARALLO A., ET AL. (1986) *The determination of air pollution abatement in Milan urban area.* In: Air Pollution Modeling and Its Application; V. De Wispelaere, F. Schiermeier, N. Gillani, eds. Plenum Press, New York.

CHRÓŚCIEL ST. (ED.) (1983) *Instructions for standard calculations of emission parameters for industrial sources* (in Polish). Technical University of Warsaw Publ., Warszawa.

DERNWENT R.G. (1988) *A better way to control air pollution.* Nature, vol. 331, February 1988, 575 – 578.

DICKERSON M.H. (1978) *MASCON – A mass consistent atmospheric flux model for regions with complex terrain.* J. Appl. Meteorology, vol 17, March 1978.

ELIASSEN A., SALTBONES J. (1983) *Modelling of long-range transport of sulphur over Europe: A two-year model run and some model experiments.* Atmos. Environment, vol 17, 1457 – 1473.

FINDLAY B.F., HIRT M.S. (1969) *An urban-induced mesocirculation.* Atmos. Environment, vol. 3, March 1969.

HANNA S.R., BRIGGS G.A., HOSKER R.P. (1982) *Handbook of Atmospheric Diffusion.* Techn. Inf. Center, U.S. Dept. of Energy.

HOLNICKI P., ŻOCHOWSKI A. (1990) *Selected Mathematical Methods in Air Quality Analysis*, (in Polish). Polish Scientific Publishers (PWN), Warszawa.

HOLNICKI P. (1990) *A multilayer model of air quality analysis*, (in Polish). Omnitech Publishers, Warszawa.

HOLNICKI P., KAŁUSZKO A. (1992) *Decision support algorithm for air quality planning by emission abatement.* Proceedings of the 15th IFIP Conference on System Modelling and Optimization, Zurich 1991, Springer-Verlag.

HOLNICKI P., KAŁUSZKO A., ŻOCHOWSKI A. (1992) *Regional/Urban Air Quality Management System.* Report of the Conteracted Study Agreement ACA-SRI (1991/92), Warszawa.

JUDA-KUCZKA K. (1987) *A three-layer model of air pollution dispersion* , (in Polish). PhD Thesis, Technical University of Warsaw, Warszawa.

MORGAN M.G., ET AL. (1986) *Technical uncertainty in quantitative policy analysis – a sulphur air pollution example.* In: Air Pollution Modeling and Its Application; V. De Wispelaere, F. Schiermeier, N. Gillani, eds. Plenum Press, New York.

O'BRIEN J.J. (1979) *A note on the vertical structure of the eddy exchange coefficient in the planetary boundary layer.* J. Atmos. Sciences, vol. 27.

SUTTON O.G. (1958) *Micrometeorology* (Russian edition). Hydroizdat Publishers, Leningrad.

ULIASZ M. (1983) *Air pollution dispersion model for regional emission control* (in Polish). Report PR8/7.2.5.3, Warsaw.

ZDANSKI A.K., KRYLOVA T.O. (1986) *Numerical modelling oil pollution dispersion in shelf region.* Report of the Computing Center Acad. of Sciences USSR, Moscow.